

T2:

Polarization and magnetic fields *Chair: Athol Kemball*

Maser polarization and magnetic fields

W. H. T. Vlemmings

Department of Earth and Space Sciences, Chalmers University of Technology, Onsala Space Observatory, SE-439 92 Onsala, Sweden

Abstract. Maser polarization observations can reveal unique information on the magnetic field strength and structure for a large number of very different astronomical objects. As the different masers for which polarization is measured, such as silicon-monoxide, water, hydroxyl and methanol, probe different physical conditions, the masers can even be used to determine for example the relation between magnetic field and density. In particular, maser polarization observations have improved our understanding of the magnetic field strength in, among others, the envelopes around evolved stars, Planetary Nebulae (PNe), massive star forming regions, supernova remnants and megamaser galaxies. This review presents an overview of maser polarization observations and magnetic field determinations of the last several years and discusses some of the theoretical considerations needed for a proper maser polarization analysis.

Keywords. masers, polarization, magnetic fields

1. Introduction

Because of their compactness, their high brightness and the fact that they occur in a wide variety of astrophysical environments, masers are excellent astrophysical probes. As the masers are often highly linearly and circularly polarized, polarization observations add fundamental information on both the masing process (such as pumping and level of maser saturation) and the physical conditions in the masing gas. With a detailed theory of maser polarization propagation, the observations can yield the strength of the magnetic field along the maser line of sight and the two-dimensional (or even three-dimensional) field structure. Consequently, they allow for a determination of the dynamical importance of the magnetic field. And, since masers are specifically suited for high angular resolution observations with interferometry instruments, the polarization observations can probe the magnetic field properties at unprecedented small scales.

In the last several years, maser polarization observations have been used to determine the strength and structure of magnetic field in the circumstellar envelopes (CSE) of Asymptotic Giant Branch (AGB) stars, high-mass star forming regions and supernova remnants (SNRs), while observations of the magnetic field strength in megamasers have also become possible. Here, I will mainly discuss results obtained since the last maser IAU symposium (IAU 242, 2007, eds. Chapman & Baan), focusing on the maser transitions in the radio-wavelength regime. In particular, in 2008, the first measurement of 6.7 GHz methanol maser circular polarization was made (Vlemmings 2008) and the considerations of its analysis are discussed. In §2, the theoretical background of maser polarization are briefly described. Recent magnetic field measurements and their consequences for related astrophysical problems involving evolved stars and high-mass star forming regions are presented in §3 and §4 respectively. §5 highlights a few further maser polarization results and finally §6 presents perspectives for future instruments and observations.

2. Background and considerations

There exists extensive literature on the theory of maser polarization, as polarization during maser amplification differs from the regular thermal emission case due to the stimulated emission process and a range of other properties of the masing process that can influence the radiation polarization characteristics. The main theoretical problem is framed by constructing the density matrix evolution and radiative transfer equations for the maser emission including the Zeeman terms (Goldreich *et al.* 1973). The Zeeman effect occurs when the degeneracy of magnetic substates is broken under the influence of a magnetic field. The magnitude of the Zeeman effect is significantly different for paramagnetic (e.g. OH) and non-paramagnetic molecules (e.g. SiO, H₂O and methanol), due to the ratio between the Bohr magneton ($\mu_B = e\hbar/2m_e c$) and the nuclear magneton ($\mu_N = e\hbar/2m_n c$). In these expressions e is the electron charge, \hbar is the Planck constant and c the speed of light. The ratio of the two ($\mu_B/\mu_N \approx 10^3$) is determined by the ratio of the electron mass (m_e) and the nucleon mass (m_N) and implies three orders of magnitudes larger Zeeman splitting for a similar magnetic field strength in the case of paramagnetic molecules compared to the non-paramagnetic ones.

A fundamental difference in the treatment of polarized maser emission exists between cases when the magnetic transitions overlap in frequency or when they are well separated. This can be defined by the splitting ratio $r_Z = \Delta\nu_Z/\Delta\nu_D$, where $\Delta\nu_Z$ is the Zeeman splitting and $\Delta\nu_D$ the Doppler line width. Typically, $r_Z \gtrsim 1$ for the paramagnetic molecule OH, while $r_Z < 1$ for the other, non-paramagnetic maser species. In the case of $r_Z > 1$ there are no theoretical ambiguities and the Zeeman components are well separated and resolved. The magnetic transitions $\Delta m_F = \pm 1$ give rise to the σ^\pm components, circularly polarized perpendicular to the magnetic field B . The transition $\Delta m_F = 0$ gives rise to the π component, linearly polarized along B . For an arbitrary angle between B and the maser propagation direction θ , the resultant components are elliptically polarized for $\theta < \pi/2$, and linearly polarized for $\theta = \pi/2$. The observed splitting of the Zeeman components directly gives the magnetic field strength $B \cos \theta$.

In the case of $r_Z < 1$, the Zeeman components overlap. The derived B strengths when $r_Z < 1$ do not only depend on the circular polarization fraction but also depend on the maser saturation level. Especially for masers that are saturated, simple assumptions with a fixed proportionality between circular polarization and magnetic field strength can lead to B being overestimated by up to a factor of 4. Theoretical work has been done both analytically and numerically with different implications for the derived magnetic field strengths (e.g. Watson 1994, Elitzur 1996, and references therein). A comparison of the different polarization theories is given by Gray (2003), who finds the numerical models can be used to accurately describe the maser polarization. In even more recent work (Dinh-V-Trung 2009) has revisited the theoretical maser calculations from first principles, avoiding the typically made assumptions that the maser radiation field is stationary and that the different spectral components are not correlated. Dinh-V-Trung (2009) finds that the numerical calculation of maser polarization (e.g. Watson 1994) are sufficient in the unsaturated and partially saturated regime.

In both Zeeman splitting cases ($r_Z < 1$ and $r_Z > 1$) there are several other properties of the maser and its surrounding medium that need to be taken into account when interpreting polarization observations. Especially at the low frequencies, Faraday rotation can make a direct connection between the polarization angle and the B -field uncertain. External Faraday rotation can cause significant vector rotation originating along the line of sight to the maser source. For instance at 1.6 GHz, a typical interstellar electron density and magnetic field strength can cause up to a full $\sim 180^\circ$ rotation towards

the W3(OH) star forming region. Additionally, internal Faraday rotation can alter the polarization characteristics of individual maser features in a source in different ways, possibly destroying any large scale structure in the linear polarization measurements (e.g. Fish & Reid 2006).

2.1. On the Zeeman splitting of methanol masers

As mentioned above, the interpretation of maser polarization depends critically on the Zeeman frequency shift in relation to the maser saturation level. The recent detection of the circular polarization of 6.7 GHz methanol masers (e.g. Vlemmings 2008; Fig. 1), has led to the need of a careful evaluation of the relevant methanol Zeeman frequency shift (Vlemmings *et al.* 2011b).

The methanol molecule is a non-paramagnetic molecule and as a result the Zeeman splitting under the influence of a magnetic field is extremely small. The split energy, ΔE_Z , of an energy level under the influence of a magnetic field, B , can be described as $\Delta E_z = g_L \mu_N M_J B$, where M_J denotes the magnetic quantum number for the rotational transition described with the total angular momentum quantum number J , B is the magnetic field strength in units of Tesla ($= 10^4$ G), μ_N is the nuclear magneton and g_L is the Landé g -factor. The Zeeman effect is determined by the Landé g -factor, which needs to be determined from laboratory spectroscopy.

In most previous publications of methanol polarization, the g -factor used to determine the magnetic field strength was based on laboratory measurements performed many years ago on a number of methanol transitions near 25 GHz methanol (Jen 1951). However, there are several caveats regarding these measurements. Firstly, g_L is an average of the true g -factor of several interacting states. Additionally, the measurements are classified as preliminary, and the exact transitions that were used are not specified. The observations were done on poorly identified transitions around 25 GHz with $\Delta J = 0$ and $K = 2 - 1$, which likely indicates it concerns the E1-type methanol maser. It is thus not impossible that an extrapolation to the 6.7 GHz $5_1 - 6_0$ A⁺ methanol transition and others transitions with different ΔJ and quantum number K is invalid.

While it is thus unclear if the g -factor determined in 1951 can be used for the 6.7 GHz methanol maser, it is the only estimate available to us at the moment. For the Zeeman splitting coefficient for the $5_1 - 6_0$ A⁺ 6.7 GHz methanol maser transition extrapolated from the laboratory measurements this implies $0.005 \text{ km s}^{-1} \text{ G}^{-1}$, an order of magnitude smaller than previously used and implying unlikely high magnetic fields of ~ 100 mG in the methanol maser region of massive star forming regions. Based on comparison with 6 GHz OH masers at similar densities, for which typical fields measured are of order ~ 10 mG, the true g -factor of methanol could be an order of magnitude larger.

Alternatively, the methanol circular polarization can be caused by non-Zeeman effects. In Vlemmings *et al.* (2011b) various different effects were investigated and ruled unlikely. The case of the rotation of the axis of symmetry for the molecular quantum states deserves some more detail here. This can occur when, as the maser brightness increases while it becomes more saturated, the rate for maser stimulated emission R becomes larger than the Zeeman frequency shift $g\Omega$. While $g\Omega \gg R$, the magnetic field direction is the quantization axis. Then, when R becomes larger than $g\Omega$, the molecules interact more strongly with the radiation field than with the magnetic field and the quantization axis changes towards the maser propagation direction. This change will cause an intensity-dependent circular polarization that mimics the regular Zeeman splitting.

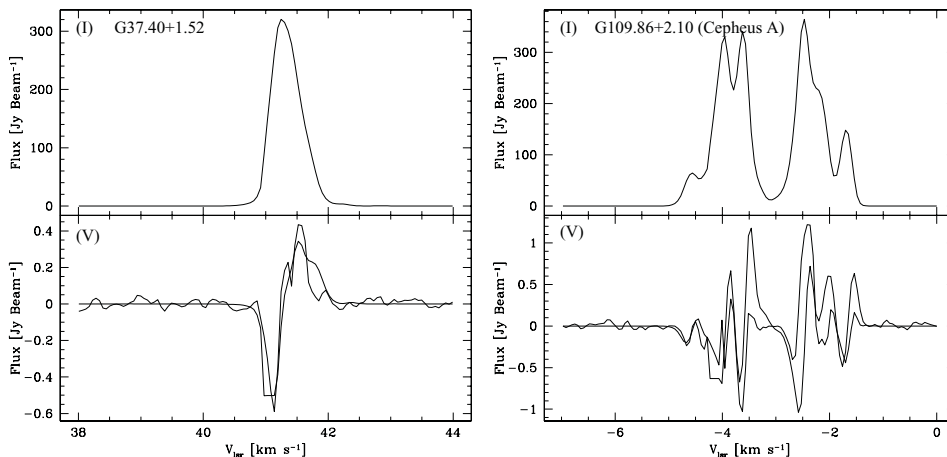


Figure 1. From Vlemmings (2008), Total intensity and circular polarization spectrum for G37.40+1.52 (left) and G109.86+2.10 (Cepheus A; right). The thick solid line in the bottom panel is best fit fractional total power derivative to the circular polarization spectrum.

From the methanol maser Zeeman splitting coefficient given above, $g\Omega \approx 0.1B[\text{mG}] \text{ s}^{-1}$ for the 6.7 GHz methanol maser. The rate for stimulated emission can be estimated using:

$$R \simeq AkT_b \Delta\Omega / 4\pi h\nu. \quad (2.1)$$

Here A is the Einstein coefficient for the maser transition, which is equal to $0.1532 \times 10^{-8} \text{ s}^{-1}$, and k and h are the Boltzmann and Planck constants respectively. The maser frequency is denoted by ν , and T_b and $\Delta\Omega$ are the maser brightness temperature and beaming solid angle. observations indicate typically $T_b \lesssim 10^{10} \text{ K}$. The beaming angle $\Delta\Omega$ is harder to estimate and decreases rapidly with increasing maser saturation level. If we very conservatively assume a maser beaming angle of $\Delta\Omega \approx 10^{-2}$, the typical maser stimulated emission $R \sim 0.04 \text{ s}^{-1}$. Thus, for a typical field strength of $\sim 10 \text{ mG}$, $g\Omega/R > 25$ and only for the most saturated masers would we expect the non-Zeeman effect to be applicable.

3. Evolved stars and planetary nebulae

Maser polarization observations are the predominant source of information about the role of magnetic fields during the late stages of stellar evolution. Most observations have focused on the masers in the CSEs of AGB stars, as OH, H₂O and SiO masers are fairly common in these sources. However, polarization observations of masers around post-AGB stars and (Proto-)PNe are becoming more common as more such sources with maser emission are found.

3.1. AGB stars & Supergiants

Recent polarization observations of CSE 1.6 GHz OH masers confirm a regular structure and few milliGauss magnetic field strength in AGB OH maser envelopes (Wolak *et al.* 2012) as found in previous observations. Recent years have also seen an increase in 22 GHz H₂O and 43 GHz SiO maser observations of Mira variables, OH/IR stars and supergiants. As the different maser species typically occur in different regions of the CSE, combining observations of all three species allows us to form a more complete picture of the magnetic field throughout the entire envelope (Fig. 2). Close to the central star, SiO maser linear

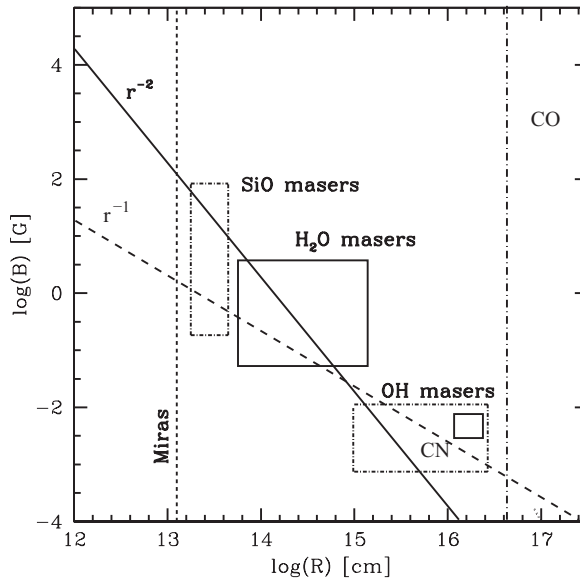


Figure 2. Magnetic field strength vs. radius relation as indicated by current maser polarization observation of a number of Mira stars. The boxes show the range of observed magnetic field strengths derived from the observations of SiO, H₂O and OH masers and thermal CN. The thick solid and dashed lines indicate an r^{-2} solar-type and r^{-1} toroidal magnetic field configuration. The vertical dashed line indicates the stellar surface. CO polarization observations will uniquely probe the outer edge of the envelope (vertical dashed dotted line).

polarization reveals an ordered B -field with a linear polarization fraction ranging up to $m_l \sim 100\%$ (e.g. Cotton *et al.* 2011, Amiri *et al.* 2012). A large single dish survey of SiO maser polarization revealed an average field strength of 3.5 G when assuming a regular Zeeman origin of the polarization, indicating a dynamically important B -field (Herpin *et al.* 2006). The observations find no specific support for other (non-Zeeman) interpretations of the polarization (e.g. Richter *et al.*, this proceedings).

Further out in the envelope, also 22 GHz H₂O maser measurements reveal significant B -fields, both around Miras and supergiants (Vlemmings *et al.* 2005, and references therein). The measured field strength is typically of the order of $\sim 100 - 300$ mG but can be up to several Gauss. The strongest field strengths are found around Mira variables, consistent with the H₂O masers occurring closer to the star. As no linear polarization has been detected thus far, describing the magnetic field shape is difficult. However, for the Supergiant VX Sgr, the complex maser structure reveals an ordered field reversal across the maser region consistent with a dipole B -field. Interestingly, the orientation of the field determined from the H₂O maser polarization is similar to the orientation of the outflow determined from other H₂O maser observations as well as the orientation of a dipole field determine from OH maser polarization. It is even similar to the direction of the SiO maser polarization measured with the Submillimeter Array (SMA) (Fig.2; Vlemmings *et al.* 2011a).

3.2. Proto-Planetary nebulae

By now, a number of P-PNe have had their magnetic fields measured using OH and H₂O masers. Similar to the magnetic field strengths around their progenitor stars, the P-PNe fields are ~ 1 mG in the OH maser region (e.g. Etoke & Diamond 2010). Single dish surveys reveal linear and circular polarization in respectively $\sim 50\%$ and $\sim 75\%$ of the

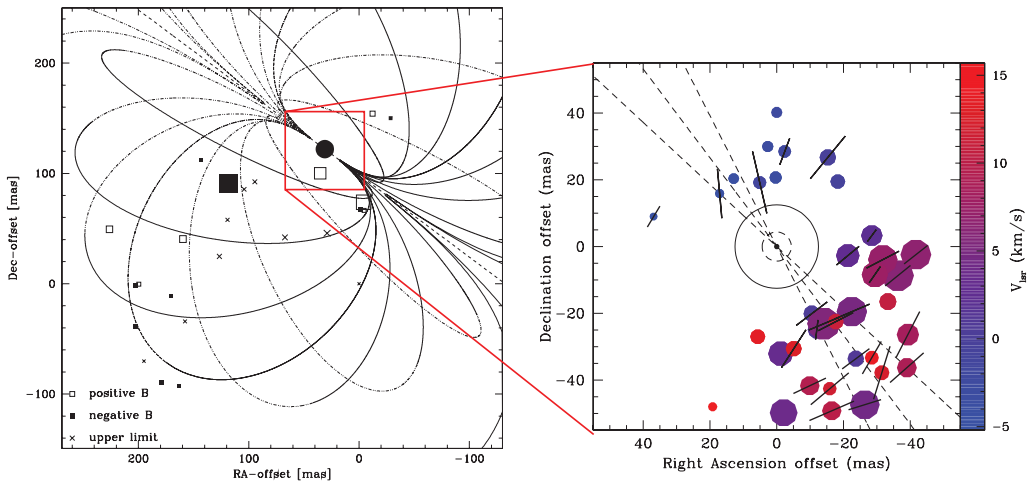


Figure 3. (left) The dipole magnetic field of the supergiant VX Sgr as determined from a fit to the H₂O maser magnetic field observations (Vlemmings *et al.* 2005). (right) Positions and polarization of the VX Sgr $v = 0, J = 5 - 4$ ²⁹SiO masers observed with the SMA (Vlemmings *et al.* 2011a). The masers spots are plotted with respect to the peak of the continuum emission. The black vectors are the observed polarization vectors scaled linearly according to polarization fraction. The long dashed inner circle indicates the star and the solid circle indicates the location of the 43 GHz SiO masers. The short dashed circle indicates the minimum radius of the ²⁸SiO masers. The dashed lines indicate the position angle and its uncertainty of the inferred orientation of the dipole magnetic field of VX Sgr observed using H₂O and OH masers (Vlemmings *et al.* 2005, Szymczak *et al.* 2001).

sources, dependent on the OH maser line (polarization is more common in the 1612 MHz OH satellite line than in the 1665 and 1667 main line masers). The polarization fraction is typically less than 15% (Szymczak & Gérard 2004).

A very small fraction of the Post-AGB/P-PNe maser stars show highly collimated H₂O maser jets (see e.g. Desmurs 2012; these proceedings). These so-called water-fountain sources are likely the progenitors of bipolar PNe and there are indications that they evolve from fairly high-mass AGB stars. The archetype of this class is W43A and polarization observations have revealed that the maser jet is magnetically collimated (Vlemmings *et al.* 2006). In addition to the observations of W43A, recent Australia Telescope Compact Array (ATCA) observations of the likely water-fountain source IRAS 15445-5449 (Pérez-Sánchez *et al.* 2011) also indicate a magnetic H₂O maser jet. The first measurement of the magnetic field strength within a few tens of AU of the binary post-AGB Rotten Egg Nebula, in the H₂O maser region entrained by the fast bipolar outflow, was also recently presented (Leal-Ferreira *et al.* 2012).

3.3. Planetary Nebulae

There are only a handful of PNe known which show maser emission, and even less of these have masers that are strong enough to provide B -field measurements from polarization observations. One of the sources that shows both OH and H₂O maser emission is the very young PNe K3-35. In this source, the OH masers indicate a B -field of a ~ 0.9 mG at 150 AU from the central object (Gómez *et al.* 2009).

3.4. Summary

Fig. 2 gives a summary of the current magnetic field measurements in CSEs of Mira stars. Although the exact relation between the magnetic field strength and distance

Table 1. Energy densities in AGB envelopes

		Photosphere	SiO	H ₂ O	OH
B	[G]	~ 50?	~ 3.5	~ 0.3	~ 0.003
R	[AU]	-	~ 3	~ 25	~ 500
		-	[2 – 4]	[5 – 50]	[100 – 10.000]
V_{exp}	[km s ⁻¹]	~ 5	~ 5	~ 8	~ 10
n_{H_2}	[cm ⁻³]	~ 10 ¹⁴	~ 10 ¹⁰	~ 10 ⁸	~ 10 ⁶
T	[K]	~ 2500	~ 1300	~ 500	~ 300
<hr/>		<hr/>		<hr/>	
$B^2/8\pi$	[dyne cm ⁻²]	10^{+2.0?}	10^{+0.1}	10^{-2.4}	10 ^{-6.4}
nKT	[dyne cm ⁻²]	10 ^{+1.5}	10 ^{-2.8}	10 ^{-5.2}	10 ^{-7.4}
ρV_{exp}^2	[dyne cm ⁻²]	10 ^{+1.5}	10 ^{-2.5}	10 ^{-4.1}	10^{-5.9}
V_A	[km s ⁻¹]	~ 15	~ 100	~ 300	~ 8

to the central star remains uncertain, the field strengths are obvious strong enough to dynamically influence the shaping of the outflow and help shape asymmetric PNe. To properly determine the possible effect of the magnetic fields, it is illustrative to study the approximate ratios of the magnetic, thermal and kinematic energies contained in the stellar wind. In Table 1 I list these energies along with the Alfvén velocities and typical temperature, velocity and temperature parameters in the envelope of AGB stars. While many values are quite uncertain, as the masers that are used to probe them can exist in a fairly large range of conditions, it seems that the magnetic energy dominates out to ~ 50 – 100 AU in the circumstellar envelope.

4. High-mass star formation

Star forming regions, and especially those forming high-mass stars, often contain a wide variety of maser species tracing many different density and temperature regimes. As was the case for evolved stars, most information on the small scale magnetic fields comes from maser polarization observations, dominated by OH maser measurements but also with an increasing number of H₂O and methanol maser observations.

4.1. OH masers

There exists a large number of OH maser polarization measurements, probing densities from ~ 10⁵ – 10⁸ cm⁻³. OH masers are often strongly polarized and as the Zeeman splitting is large, observations of the separate σ^+ and σ^- components directly yields a magnetic field strength. Observations of the 100% linearly polarized π -component are extremely rare however, likely due to magnetic beaming and the overlap of several differently polarized masers along the line of sight (Fish & Reid 2006). The measured field strengths are typically around ~ 1 mG. Most of the recent OH maser work has been performed by Caswell *et al.* (2009, 2011), including observations of the polarization of 6 GHz OH masers. These results seem to imply a relation between the Galactic magnetic field and that measured in the OH maser region.

4.2. H₂O masers

After the first discovery of interstellar H₂O maser Zeeman splitting by Fiebig & Güsten (1989) using single dish observations, there have been an increasing number of higher

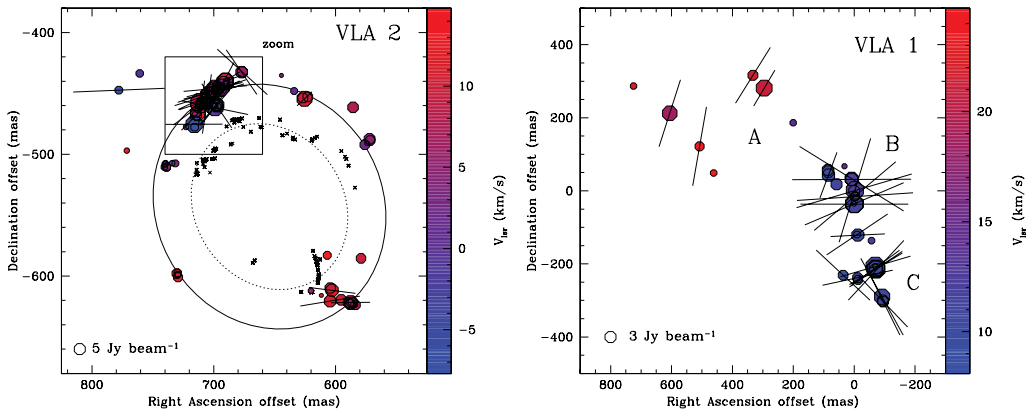


Figure 4. From Surcis *et al.* (2011). The H₂O masers of VLA2 (left) and VLA1 (right) in the massive star forming region W75N. The line segments denote the polarization fraction and direction and the maser features are scaled according to their flux. In the left panel, the ellipses indicate the expansion of the maser ring from previous observations (crosses, Torrelles *et al.* (2003))

spatial resolution circular polarization observations confirming the earlier results (e.g. Sarma *et al.* 2001). These observations typically reveal *B*-field strengths between 15 and 150 mG at densities of $n_{\text{H}_2} = 10^8 - 10^{11} \text{ cm}^{-3}$. In addition to the circular polarization, low levels of linear polarization (typically $\lesssim 2\%$) are also observed in star forming regions. While often structure in the *B*-field direction is detected, the observations show rapid changes of direction over small scales (see Fig. 4).

In addition to providing information on the magnetic field strength and structure, full maser polarization radiative transfer modeling can also provide important information on other physical quantities of the masing gas. In particular, the observations by Surcis *et al.* (2011) have revealed striking differences of intrinsic line-width and hence either turbulent widths or temperatures around two sources, VLA1 and VLA2, in the W75N massive star forming region. These sources are thought to represent two different evolutionary stages of proto-stars.

4.3. Methanol masers

The 6.7 and 12 GHz methanol masers are some of the most abundant masers in high-mass star forming regions. After the initial presentation of their polarization, the last few years have seen an increasing number of publications on polarimetric methanol maser studies (e.g. Vlemmings *et al.* 2006, 2008, 2011, Dodson 2008, Stack & Ellingsen 2011). In particular, 6.7 GHz methanol maser observations with MERLIN have shown that the magnetic field is likely regulating the infall on the circumstellar disk in the Cepheus A region (Vlemmings *et al.* 2010). The methanol maser polarimetry has now also been extended to higher frequency class-I masers (e.g. Sarma *et al.* 2009, and these proceedings). While as described above, the methanol circular polarization cannot yet be used to determine the magnetic field strength, the linear polarization has shown large scale magnetic field structures that are consistent with magnetic field observations at other frequencies (e.g. Surcis *et al.* 2009, and these proceedings).

4.4. Summary

The recent magnetic field observations, and in particular those of methanol, indicate a clear relation between the maser derived magnetic field direction and that of known

outflows and/or circumstellar toroidal structures. Additionally, they often show a good agreement with dust polarization measurements at lower resolution. This indicates that maser do not, as occasionally thought, probe isolated pockets of magnetized gas, but rather are indeed good probes of the magnetic field in star forming regions.

The B -field measurements of both masers and non-maser observations as a function of number density seem to indicate that the field strength follows an approximate $B \propto n^{0.5}$ density scaling law over an enormous range of densities. This implies that the magnetic field remains partly coupled to the gas up to the highest number density. However, above $n \sim 10^8 \text{ cm}^{-3}$, the shock excited H_2O maser are short-lived (with a typical lifetime $\tau_m \sim 10^8 \text{ s}$) compared to the typical adiabatic diffusion timescale at the highest densities ($\tau_d \sim 10^9 \text{ s}$), and in the non-masing gas of similar high densities, magnetic field strengths should be lower due to the adiabatic diffusion. Still, the maser B measurements strongly indicate a dynamical importance of magnetic fields during the high-mass star formation process, especially in shaping outflows and jets.

5. Further maser polarization studies

Besides the evolved stars and star forming regions, masers are found in several other types of sources, such as supernova remnants and megamaser galaxies. However, there have been few recent publications on polarization from these sources. However, work is progressing on the measurement of OH megamaser polarization such as presented by Robishaw *et al.* (2008). These authors measured the Zeeman splitting of OH megamaser emission at 1667 MHz from five ULIRGs using the Arecibo and Green Bank Telescope. They found line-of-sight magnetic field strengths ranging from ~ 0.5 to 18 mG, similar to those measured in Galactic OH masers. They infer that this suggests that the local process of massive star formation in ULIRGs occurs under similar conditions as in the Galaxy.

Finally, besides the maser species discussed above, hydrogen recombination line masers have also been shown to display polarization. This is described further in Thum *et al.* (these proceedings).

6. Future perspectives

The wealth of new maser polarization observations over the last few years has clearly demonstrated the relevance of masers in the study of Galactic as well as extra-galactic magnetic fields. Especially methanol maser polarization observations have shown their enormous potential. In the near future, maser polarization will be an important goal in the observations with the upgraded EMERLIN and EVLA and also the VLBI observations with the EVN and VLBA will make great strides in detailed imaging of circumstellar and protostellar magnetic fields. At the higher maser frequencies, ALMA will provide a further step when its polarimetric capabilities are offered (as shown by Pérez-Sánchez *et al.*, these proceedings). Additionally, SMA and ALMA high resolution dust polarization observations will also close the gap between the small scale maser magnetic field measurements and the very large scale single dish dust polarization observations.

Acknowledgements

WV acknowledges support by the Deutsche Forschungsgemeinschaft (DFG) through the Emmy Noether Research grant VL 61/3-1.

References

- Amiri, N., Vlemmings, W. H. T., Kembell, A. J., & van Langevelde, H. J. 2012, *A&A*, 538, A136
- Caswell, J. L., Kramer, B. H., & Reynolds, J. E. 2009, *MNRAS*, 398, 528
- Caswell, J. L., Kramer, B. H., & Reynolds, J. E. 2011, *MNRAS*, 415, 3872
- Cotton, W. D., Ragland, S., & Danchi, W. C. 2011, *ApJ*, 736, 96
- Dinh-v-Trung 2009, *MNRAS*, 399, 1495
- Dodson, R. 2008, *A&A*, 480, 767
- Elitzur, M. 1996, *ApJ*, 457, 415
- Etoka, S. & Diamond, P. J. 2010, *MNRAS*, 406, 2218
- Fiebig, D. & Güsten, R. 1989, *A&A*, 214, 333
- Fish, V. L. & Reid, M. J. 2006, *ApJS*, 164, 99
- Goldreich, P., Keeley, D. A., & Kwan, J. Y. 1973, *ApJ*, 179, 111
- Gómez, Y., Tafuya, D., Anglada, G., *et al.* 2009, *ApJ*, 695, 930
- Gray, M. D. 2003, *MNRAS*, 343, L33
- Herpin, F., Baudry, A., Thum, C., Morris, D., & Wiesemeyer, H. 2006, *A&A*, 450, 667
- Jen, C. K. 1951, *Physical Review*, 81, 197
- Leal-Ferreira, M. L., Vlemmings, W. H. T., Diamond, P. J., *et al.* 2012, arXiv:1201.3839
- Pérez-Sánchez, A. F., Vlemmings, W. H. T., & Chapman, J. M. 2011, *MNRAS*, 418, 1402
- Robshaw, T., Quataert, E., & Heiles, C. 2008, *ApJ*, 680, 981
- Sarma, A. P., Troland, T. H., & Romney, J. D. 2001, *ApJ*, 554, L217
- Sarma, A. P. & Momjian, E. 2009, *ApJ*, 705, L176
- Stack, P. D., & Ellingsen, S. P. 2011, *PASA*, 28, 338
- Surcis, G., Vlemmings, W. H. T., Dodson, R., & van Langevelde, H. J. 2009, *A&A*, 506, 757
- Surcis, G., Vlemmings, W. H. T., Curiel, S., *et al.* 2011, *A&A*, 527, A48
- Szymczak, M., Cohen, R. J., & Richards, A. M. S. 2001, *A&A*, 371, 1012
- Szymczak, M. & Gérard, E. 2004, *A&A*, 423, 209
- Torrelles, J. M., Patel, N. A., Anglada, G., *et al.* 2003, *ApJ*, 598, L115
- Vlemmings, W. H. T., van Langevelde, H. J., & Diamond, P. J. 2005, *A&A*, 434, 1029
- Vlemmings, W. H. T., Diamond, P. J., & Imai, H. 2006a, *Nature*, 440, 58
- Vlemmings, W. H. T., Harvey-Smith, L., & Cohen, R. J. 2006c, *MNRAS*, 371, L26
- Vlemmings, W. H. T. 2008, *A&A*, 484, 773
- Vlemmings, W. H. T., Surcis, G., Torstensson, K. J. E., & van Langevelde, H. J. 2010, *MNRAS*, 404, 134
- Vlemmings, W. H. T., Humphreys, E. M. L., & Franco-Hernández, R. 2011, *ApJ*, 728, 149
- Vlemmings, W. H. T., Torres, R. M., & Dodson, R. 2011, *A&A*, 529, A95
- Watson, W. D. 1994, *ApJ*, 424, L37
- Wolak, P., Szymczak, M., & Gérard, E. 2012, *A&A*, 537, A5